

ABC 11 - Program – DAY 3

Lecture theatre 505-011, Grafton Campus

5th Dec 2018 MBSANZ18 & ABC11 Shared Day on Mechanobiology AA	
8.00am	Registration opens – Atrium of Building 505
8.30am to 9.00am	Mihi - a traditional Maori welcome MBSANZ18 and 10th Annual Mechanobiology Symposium Opening
9.00am to 11.05am Session Chairs: Dr Sue McGlashan and A/Prof Ashvin Thambyah	MECHANOBIOLOGY AND THE MATRIX Invited Speakers: Professor Toshiro Ohashi – Hokkaido University, Hokkaido, Japan INVESTIGATION OF ENDOTHELIAL MECHANOTRANSDUCTION MECHANISM: MECHANICAL PROPERTIES OF PRIMARY CILIA Professor Peter Torzilli – Cornell University & Hospital for Special Surgery, NY, USA SOFT TISSUE BIOMECHANICS AND MECHANOBIOLOGY OF ARTICULAR CARTILAGE Scientific presentations <ul style="list-style-type: none"> • A model of bone mechanostat directed by osteocytes mechanosensation – Madge Martin (Queensland University of Technology) • Ultrastructural characterisation of the osteocyte lacunar-canalicular network during aging – mechanobiological implications – Peter Pivonka (Queensland University of Technology) • Towards cellular epidemiology of degenerative diseases using geographic information systems, multisem and machine learning approaches – Anton Nathanson (University of New South Wales) • The impact of joint injury on the development of meniscal pathology and its association with OA in ACL deficient knees – Carina Blaker (University of Sydney) • The extracellular matrix facilitates mechanical activation of epithelial Na⁺ channel in response to shear force to regulate blood pressure – Martin Fronius (University of Otago) • Tenocyte shape, and the expression of cytoskeleton and matrix remodelling genes, are altered when cells are cultured on degenerated ECM – David Musson (University of Auckland)

A MODEL OF BONE MECHANOSTAT DIRECTED BY OSTEOCYTES MECHANOSENSATION

M. Martin^{1,2}, V. Sansalone², D. M. L. Cooper⁴, M. Forwood⁵, L. Bonewald⁶, P. Pivonka¹

¹School of Chemistry, Physics and Mechanical Engineering, Queensland University of Technology, QLD, Australia

²Université Paris-Est, Laboratoire Modélisation et Simulation Multi Echelle, Créteil, France

³Department of Anatomy & Cell Biology, University of Saskatchewan, SK, Canada

⁴School of Medicine, Griffith University, QLD, Australia

⁵School of Dentistry, University of Missouri Kansas City, MS, USA

INTRODUCTION

The mechanostat is a concept that was introduced by Frost in 1987 [1], referring to the feedback loop between the evolution of the tissue and the mechanical environment. It is well accepted now that osteocytes play a key role in controlling this feedback, i.e., they sense mechanical loading and respond, in particular by changing their production of nitric oxide (NO) and sclerostin (Scl). Based on previous studies [2,3], we use here a micro-mechanical model to translate the loading on bone porous architecture resulting in bone matrix strains “felt” by osteocytes which in turn produce biochemical signals which serve as a local feedback for cells involved in bone remodeling.

METHOD

We modelled the effects of osteocytes’ signalling on the bone cell population by modelling the regulatory actions of Scl and NO. The present model relies on the description of the regulation mechanisms at stake in bone remodeling at the cellular level. To this end, in line with Pivonka et al. [2], we use sigmoidal functions to account for inhibitory and stimulating actions of ligands and mechanical loading on cellular activity.

Sclerostin binds competitively to LRP5/6 receptors, inhibiting Wnt signaling which drives bone formation by the osteoblastic cells. Nitric oxide regulates the RANKL/OPG ratio, acting on osteoclast precursors differentiation. The biochemical regulation of the population of active bone cells determines the change in porosity, therefore ensuring the “closing” of the feedback loop via the micromechanical model.

We calibrated the model to reproduce bone loss induced by a space flight and the adaptation to hormonal changes due to post-menopausal osteoporosis (PMO). Finally, we simulated the effects of a glucocorticoid treatment by a decrease in osteocyte density in the bone matrix.

RESULTS

Bone loss due to disuse was not impacted by the Wnt pathway, while its inactivation causes a major increase in bone loss in case of PMO. Figure 1 depicts how the

decrease in osteocyte density influences the evolution of bone volume fraction. Here, glucocorticoid (GC) treatment leads to a diminished inhibition of both the Wnt and the RANKL pathway and therefore an increase of the bone turnover resulting in a shift of the homeostatic state towards a higher porosity.

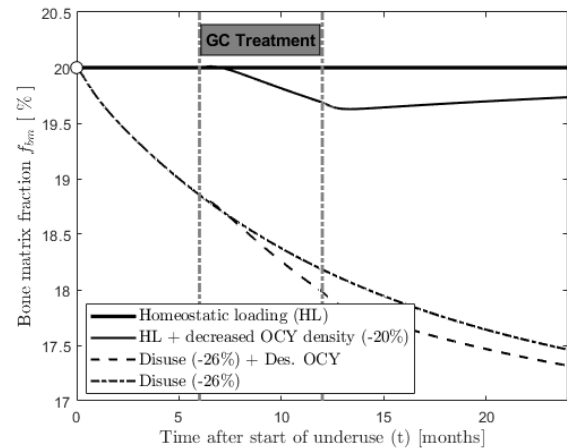


Figure 1. Evolution of bone volume fraction under: homeostatic loading (solid), mechanical disuse (dashed), and GC treatment starting after 6 months.

CONCLUSIONS

Formulating competitive binding reactions consistently as well as including major signaling molecules produced by osteocytes due to mechanobiological stimuli enables to reproduce anabolic and catabolic responses in bone remodeling. Our numerical simulations show that mechanostat anabolic and catabolic regulatory mechanisms are mutually exclusive. Finally, reduced osteocyte sensitivity offsets the mechanostat set point and diminishes mechanobiological feedback.

REFERENCES

- Frost, H. Anat Rec 219, 1-9, 1987.
 - Pivonka, P. Bone 43(2), 249–263, 2008.
 - Scheiner, S. Comput Meth Appl Mech Eng 254, 181–196, 2013.
- Madge Martin madge.martin@u-pec.fr

ULTRASTRUCTURAL CHARACTERISATION OF THE OSTEOCYTE LACUNAR-CANALICULAR NETWORK DURING AGING – MECHANOBIOLOGICAL IMPLICATIONS

L.S. Hart¹, A.M. Ashique¹, C.D.L. Thomas², J.G. Clement², S. Scheiner³, C. Hellmich³, D.M.L. Cooper¹, P. Pivonka⁴

¹University of Saskatchewan, Saskatoon, Canada; ²University of Melbourne, Melbourne, Australia; ³Vienna University of Technology, Vienna, Austria;

⁴Queensland University of Technology, Brisbane, Australia.

INTRODUCTION

Osteocytes, the most abundant bone cells, play a central role in maintaining bone health by regulating bone remodeling, calcium homeostasis and mechanotransduction. Osteocytes and their dendritic extensions reside within hollowed cavities in the bone matrix called lacunae and canaliculi, respectively. Aberrant osteocyte communication and reduction in nutrient supply during aging may cause these cells to die or adversely influence their role in regulating bone matrix bone matrix maintenance, leading to osteoporosis.

In this contribution, we investigate the age-related changes of the 3D lacunar-canalicular network (LCN) in the mid-cortical region of the human femoral shaft. Additionally, we utilize a two-scale porosity poroelastic model to compute changes in pore pressure in the osteocyte lacunae during aging.

METHOD

Human femoral cortical bone samples were obtained post-mortem from female donors (Young: N=5, 20-23 yrs; Aged: N=5 70-86 yrs) and represent the same subset of samples used for 2D areal analysis of the LCN [1]. The femora used in this study are part of the Melbourne Femur Research Collection (MFRC)[X].

All samples were stained with 1% fluorescein isothiocyanate isomer I (FITC; Sigma Aldrich, Oakville, ON) as previously described. The cortical sections were then imaged with a Zeiss LSM710 confocal laser scanning microscope (Carl Zeiss Canada, North York, ON, Canada). Confocal image z-stacks underwent auto local mean thresholding (radius = 50, parameter 1 = -30) to form binary images which were then despeckled (ImageJ, National Institutes of Health). The z-stacks were reconstructed using AMIRA 3D 6.0 (FEI Software) to generate volume renderings.

In order to put the age-related changes of the osteocyte LCN into a mechanobiological context, we utilize the poroelastic model developed by Scheiner et al. 2016 [2]. This model allows, based on a physiological loading of bone tissue, to compute the hydrostatic pressure in both the bone vascular and lacunae pores.

RESULTS

Our imaging results indicate that both lacunar size and canalicular volume are significantly affected during aging (Fig.1 A, B). In examining the canaliculi microarchitecture in detail, the skeletonized canalicular network length in aged women is decreased by 45% and the number of canalicular branching points was decreased by 50% (Fig.1 C).

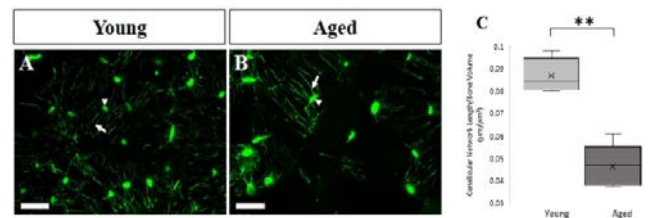


Figure 1. LCN from a 23 yr old (A) and 74 yr old (B) women using confocal microscopy imaging (scale bar 30 μ m). (C) Box plot of canalicular network length in young and old.

Using the developed poromechanical model we predict that reduction of the lacunae porosity and increase of vascular porosity during aging leads to an increase in lacunae pressure.

CONCLUSIONS

Our imaging results clearly demonstrate disruption of the LCN during aging. Particular reduction of canaliculi may lead to osteocyte apoptosis due to loss of nutrients and oxygen. However, our computational results indicate that changes of osteocyte mechanical environment may not be a driver for catabolic bone remodeling. Furthermore, this poroelastic model also shows that mechanical loading gives rise to vascular pore pressures that may be sensed by other bone cells. These mechanisms can be taken into account in state-of-the-art models of bone remodeling in order to investigate the effects of osteoporosis [5].

REFERENCES

- [1] Carter, Y. J. *Anatomy* 225(3), 328-36, 2014.
- [2] Scheiner, S. *BMMB* 15(1), 9-28, 2016.

*Prof Peter Pivonka: peter.pivonka@qut.edu.au

TOWARDS CELLULAR EPIDEMIOLOGY OF DEGENERATIVE DISEASES USING GEOGRAPHIC INFORMATION SYSTEMS, MULTISEM AND MACHINE LEARNING APPROACHES

A.D. Nathanson [1], A. Srikantha [2], M. Carnell [3], D. Zeidler [2], C. Wojek [2], M.L. Knothe Tate [1].

[1] Graduate School of Biomedical Engineering, UNSW Sydney, Australia; [2] Zeiss Microscopy GmbH, Oberkochen, Germany; [3] Biomedical Imaging Facility, UNSW Sydney, Australia

INTRODUCTION

The paucity of rapid throughput imaging technologies that allow for seamless bridging of structure-function relationships across length scales (10^{-2} to 10^{-9} m) has stymied the study of degenerative processes associated with ageing and disease. The combination of geospatial approaches using multibeam scanning electron microscopy (MultiSEM) and the Google Maps JavaScript API, have enabled cutting-edge cellular connectomics studies of ageing human tissues, from bone to brain [1-4].

METHOD

As a proof-of-principle study to elucidate the relationship between bone and cell health in the human femoral neck, the Google JavaScript API was used to enable labelling of landmarks on a navigable map (Figure 1). A blinded observer marked blood vessel edges, viable and pyknotic osteocytes. This coordinate-based mapping enabled testing of specific hypotheses related to bone health in terms of osteocyte viability, transport path distances, and network relationships. While initially adequate, this manual method is not conducive to the pipeline scalability necessary for the magnitude of current datasets (>10TB).

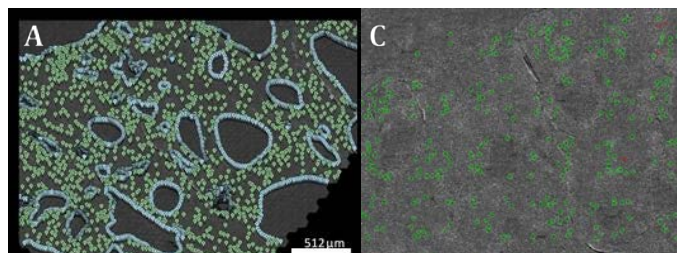


Figure 1. Left - Manual pin dropping using the Google Maps API identifying key features such as osteocytes (green) and blood vessels (blue). Right - Automatic detection using YOLO machine learning neural network (v2) detecting healthy (green) and unhealthy (red) osteocytes.

Automated object detection algorithms such as the You Only Look Once (YOLO) neural network [5] facilitate rapid throughput diagnostic assessment of imaging datasets, also mitigating the effects of observer bias. Initially, YOLO was trained for automated osteocyte detection, using 629 annotated cells, which were further augmented to 10^6 examples through variation by rotation, scale and contrast. Unseen images were then processed with YOLO and automatically detected objects were identified by bounding boxes. Latest testing (Figure 1 – Right) of the YOLO algorithm has proved successful in detecting osteocytes in a complete cross-section of the human femoral neck in <100hrs,

and early hypotheses have begun testing.

RESULTS

Initially, interest in the relationship between the path distance between all osteocytes detected using the YOLO algorithm. Previously [2], manual pinning using the Google Maps JavaScript API had revealed a relationship between osteocytes and the nearest healthy osteocyte. This investigation was furthered to include the relationship from each osteocyte (whether healthy or pyknotic) to all others per sample. Results demonstrate strong homogeneous networks of cell connectivity in this sample, implicating cell network connectivity in osteocyte survival in osteoarthritis.

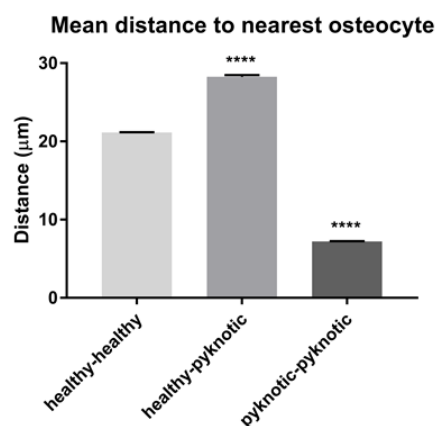


Figure 2. Mean distance to the nearest osteocyte is presented, comparing healthy- to-healthy connections ($n=158,905$), healthy-to-pyknotic connections ($n=12,986$) and pyknotic-to-pyknotic connections ($n=34,288$). Kruskal-Wallis with Dun's multiple comparisons test, ****= $p<0.0001$ compared to healthy-healthy connection.

CONCLUSIONS

These results demonstrate a clear link between the osteocyte connection network and cell health-type in a human femur with osteoarthritis. Further work is required to elucidate the exact nature of these networks, as well as investigation whether manipulations to these networks can alter disease epidemiology.

REFERENCES

- [1] Knothe Tate. Science 2017
- [2] Knothe Tate *et al.* Adv. Healthcare Mat. 5, 1840-1843, 2017
- [3] Pereira *et al.* PLoS Comp. Biol. 12, 1-18, 2017
- [4] Eberle *et al.* J. Microscopy 259, 114-120, 2015
- [5] Redmon *et al.* Proc IEEE Conference Computer Vision Pattern Recognition 2015

Anton Nathanson – a.nathanson@unsw.edu.au
Graduate School of Biomedical Engineering
Level 5, Samuels Building (F25)
UNSW Sydney, 2052, Australia

The impact of joint injury on the development of meniscal pathology and its association with OA in ACL deficient knees

Carina Blaker^{1,3}, Hadrian Platzer^{1,2}, Cindy Shu¹, Elizabeth Clarke³ and Christopher Little¹

¹*Raymond Purves Bone and Joint Research Laboratories, Institute of Bone and Joint Research, Kolling Institute, Northern Sydney Local Health District, Sydney Medical School Northern, University of Sydney, St. Leonards, NSW, Australia*

²*Department of Orthopaedics, Trauma Surgery and Paraplegiology, Heidelberg University Hospital, Heidelberg, Germany*

³*Murray Maxwell Biomechanics Laboratory, Institute of Bone and Joint Research, Kolling Institute, Northern Sydney Local Health District, Sydney Medical School Northern, University of Sydney, St. Leonards, NSW, Australia*

Introduction: Meniscal pathology is commonly associated with anterior-cruciate-ligament (ACL) injuries and substantially increases the odds of osteoarthritis (OA) following ACL injury. However, the mechanisms driving meniscal degradation and OA progression after ACL injury remain unclear. The structural and molecular progression of meniscal pathology was investigated in 2 mouse models of ACL injury with known differences in OA outcomes: surgical ACL transection (ACLT) versus mechanical ACL rupture (ACLR).

Methods: Ten-week-old, male C57BL/6 mice were assigned to ACLT, ACLR, sham surgery or un-injured. At 1, 2, 4 or 8 weeks post-injury, joints were harvested for histology (n=7) or gene expression (ACLT, ACLR: n=5; un-injured, sham: n=2, pooled samples). Quantitative PCR was performed separately in medial and lateral menisci, for key molecules implicated in meniscal and wider joint pathology.

Results: Significant pathology occurred in both medial and lateral menisci of ACL-injured joints: medial > lateral and correlated with medial tibiofemoral OA pathology only in ACLR. Significant upregulation of meniscal *Acan*, *Col2a1*, *Col10a1*, *Mmp9*, and *Mmp13* was specifically associated with ACL injury but not the model; medial generally > lateral. Increased *Acan* and *Col2a1* preceded maximal meniscal pathology, while *Col10a1*, *Mmp9*, and *Mmp13* generally increased over time in both ACL injury models. Other genes (*Col1a1*, *Adamts4*, *Mmp2*, *Lox*, *IGF*, *Il1b*) were similarly regulated in ACL-injured and Sham joints.

Conclusion: The onset of meniscal pathology was associated with more rapid/severe OA following mechanical ACL rupture. A number of specific meniscal molecular changes may be predictive of development of meniscal pathology and medial compartment OA.

The extracellular matrix facilitates mechanical activation of epithelial Na⁺ Channel in response to shear force to regulate blood pressure

Martin Fronius¹, Zoe Ashley¹, Jan-Peter Baldin¹, Daniel Barth¹ and Fenja Knöpp²

¹*Department of Physiology, University of Otago, Dunedin, New Zealand*

²*Excellence Cluster Cardiopulmonary System, University Giessen, Giessen, Germany*

Introduction: Healthy arteries sense and respond to shear force and impairment of this response is a hallmark of vascular dysfunction. Evidence underlines a role of the extracellular matrix (ECM) of arteries for this process. The epithelial Na⁺ channel (ENaC) in conjunction with the ECM are emerging candidates for this role. ENaC is regulated by shear force and expressed in the vasculature. Aim of our research is to reveal how the ECM and ENaC senses shear force to regulate arterial blood pressure.

Methods: Whole cell currents of human ENaC in response to shear force were recorded in *Xenopus* oocytes. Pressure myography on freshly isolated carotid arteries from C57BL/6 mice was performed to characterise ENaC-mediated effects on arterial diameter in response to shear force. ECM components (hyaluronic acid or heparan sulfate) were enzymatically degraded by hyaluronidase or heparanase and currents/changes in vessel diameter were recorded.

Results: In Oocytes expressing human ENaC an increased inward was observed in response to shear force (SF) that was not present in presence of amiloride (ENaC inhibitor). Degradation the ECM of hyaluronidase or heparanase impaired the SF-mediated effects of expressed ENaC. In isolated carotid arteries of mice similarly the response to intraluminal flow was impaired and this was also associated with an impaired amiloride responsiveness.

Conclusion: The ability of ENaC to sense shear force depends on an intact ECM since its degradation impairs the response to SF. Our evidence suggests that the ECM and ENaC form a shear force sensitive complex that contributes to blood pressure regulation.

Tenocyte shape, and the expression of cytoskeleton and matrix remodelling genes, are altered when cells are cultured on degenerated ECM

David Musson¹, Sophia Leung¹, Mei Lin Tay¹, Nicola Dalbeth¹, Dorit Naot¹ and Jillian Cornish¹

¹*Bone & Joint Research Group, Department of Medicine, University of Auckland, New Zealand*

Introduction: Tenocytes reside and elongate between highly organised arrangements of tendon matrix. During disease, tendon matrix is severely altered, which affects the microenvironment these cells experience. It is currently unknown how these changes affect tenocyte behaviour. We have created an *in vitro* model which mimics different stages of tendon degeneration in order to study cell responses to diseased ECM.

Methods: Human tenocytes were seeded onto slices of decellularised bovine tendon which mimic healthy and increasingly degenerative states (created by enzymatic activity), for 24hrs and 48hrs. Cell shape was determined from confocal images using ImageJ analysis. Changes in expression of tenocyte-like and non-tenocyte genes were assessed with real-time PCR. PCR gene arrays were also run to identify mechanisms of response to degenerated ECM. For all analyses, three independent experiments were carried out with cells from three different patients.

Results: Tenocytes cultured on degenerated tendon had increased cell area and a reduction in aspect ratio/cell elongation. They also had reduced expression of scleraxis (a key tenocyte transcription factor), and increased expression of cebpb (a regulator of fat cells). PCR array data showed that the expression of 38 genes related to cytoskeletal organisation were downregulated in cells on degenerated slices, while 5 different MMPs were upregulated in cells grown on degenerated slices.

Conclusion: We have shown that tenocytes respond to degenerative changes in the ECM by becoming less tenocyte-like, by morphologically changing, and by increasing the expression of genes related to matrix remodelling. These factors would all contribute to tendon disease pathology.

ABC 11 - Program – DAY 3

Lecture theatre 505-011, Grafton Campus

5th Dec 2018

MBSANZ18 & ABC11 Shared Day on Mechanobiology AA

<p>11.35am to 1.15pm Session Chairs: Dr Kathryn Stok and Dr Sophia Leung</p>	<p>MECHANOBIOLOGY TOOLBOX</p> <p>Invited Speakers</p> <p>Associate Professor Tim Woodfield – University of Otago, Christchurch, New Zealand 3D BIOPRINTING AND BIOASSEMBLY FOR REGENERATIVE MEDICINE OF MUSCULOSKELETAL TISSUES</p> <p>Associate Professor Kris Kilian – University of New South Wales, Sydney, Australia HYDROGEL MICROENGINEERING TO DECIPHER ‘MATRIX STRUCTURE-CELL FUNCTION’ RELATIONSHIPS</p> <p>Scientific presentations</p> <ul style="list-style-type: none"> • Quantifying birefringence in the bovine model of early osteoarthritis using polarisation-sensitive optical coherence tomography and mechanical indentation – Matthew Goodwin (University of Auckland) • Stiffness gradient GelMa hydrogel for 2D and 3D stem cell mechanobiology – Yu Suk Choi (University of Western Australia) • Improving chondrogenesis of equine umbilical cord blood-mesenchymal stem cell in three-dimensional hydrogel by synergistic control of chemical and mechanical cues – Xiaolin (Stephen) Cui (University of Otago) • Renal fibrosis in human kidney organoids – Veronika Sander (University of Auckland)
--	--

QUANTIFYING BIREFRINGENCE IN THE BOVINE MODEL OF EARLY OSTEOARTHRITIS USING POLARISATION-SENSITIVE OPTICAL COHERENCE TOMOGRAPHY AND MECHANICAL INDENTATION

Matthew Goodwin¹, Ashvin Thambyah², Frederique Vanholsbeeck¹

1) The Dodd-Walls Centre for Photonic and Quantum Technologies, Department of Physics,

2) Department of Chemical and Materials Engineering,

The University of Auckland. Private Bag 92019, Auckland, New Zealand.

INTRODUCTION

Osteoarthritis (OA) is a debilitating disease that affects articulating joints, in which there is a gradual wearing away of the aneural cartilage covering the bone ends, resulting in pain. The intrinsic repair capability of articular cartilage is highly limited and, once exhausted, destruction of the extracellular matrix (ECM) ensues. Microscale ECM changes in association with subtle articular surface (AC) integrity have been shown to be one of the earliest signs of cartilage degeneration [1]. An exciting prospect is that such changes may be used as a structural marker for the initiation and progression of OA. The challenge for most OA researchers, especially in the imaging domain, would be to develop ways in which this early and very mild cartilage degeneration is detected. Polarisation-Sensitive Optical Coherence Tomography (PS-OCT) is a non-invasive, micron scale, label free imaging modality. PS-OCT has the ability to detect tissue birefringence, a key indicator of collagen structural organisation. By combining PS-OCT and mechanical indentation we can detect and quantify the early degenerative changes associated with OA onset.

METHOD

Cartilage-on-bone samples were cut from bovine patella that exhibited G0, G1, or G2 degeneration when stained with India ink [2]. The samples were subject to a creep-loading at 4.5MPa and were allowed to reach equilibrium before the tissue was chemically fixed under load to fix the tissue's deformed state. Mild decalcification was then carried out and the cartilage-on-bone samples were then cryosectioned to quantify the level of cartilage degeneration at the microscale, using differential interference contrast microscopy [1]. Following cryosection, the remaining sample blocks were imaged using an in-house built swept-source PS-OCT system which has a central wavelength of 1310nm, bandwidth of 100 nm, a 50 kHz sweep rate, and average output power of 35 mW. The system has an axial resolution of 10 μm in air according to the spectrum and a lateral resolution of 20 μm . MATLAB was used to calculate the retardation gradient, a measure of the birefringence strength.

RESULTS

There is a statistically significant relationship between the retardation gradient and the extent of OA progression ($P < 0.001$) when imaging following mechanical indentation (Fig 1).

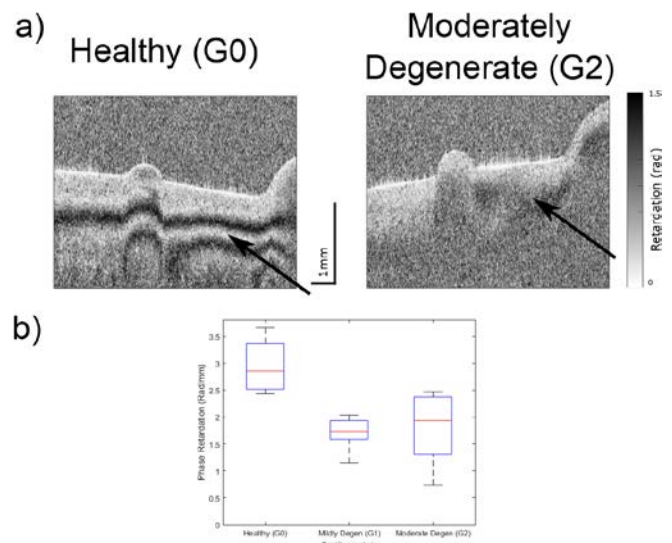


Figure 1 - a) Phase images from indented cartilage. Healthy cartilage (G0) exhibits strong birefringent banding patterns (black arrows) which are reduced with increasing degeneration (G1, G2). b) Quantitative results shows that healthy cartilage has a significantly larger retardation gradient than degenerate cartilage.

CONCLUSIONS

We have demonstrated that differentiation of healthy from early degenerate cartilage using PS-OCT is possible. However, in order to observe any differences the cartilage samples must be mechanically compressed and imaged in an 'active state'.

REFERENCES

- [1] Thambyah, A. J. mechanical behavior biomedical materials 5, 206–215 (2012).
- [2] Outerbridge, R, J Bone Jt. Surg Br 43 (1961). Matthew Goodwin (m.goodwin@auckland.ac.nz)

Stiffness gradient GelMa hydrogel for 2D and 3D stem cell mechanobiology

Yu Suk Choi¹, Luke Major¹ and Claire Kim¹

¹*School of Human Sciences, University of Western Australia, Perth, WA, Australia*

Introduction: The relationship between mechanomarkers and tissue stiffness has been screened using 2D hydrogel platforms with discontinued stiffness ranges (e.g. soft vs. stiff). However, recently studies have suggested the dimensionality of ECM and resulting cell spreading may dictate cell mechanotransduction in 3D differently to 2D.

Methods: To improve our understandings of mechanotransduction, we developed a reliable method to generate stiffness gradient hydrogels with continuous linear gradient that can be used as 2D and 3D (potential to be 4D with on-demand stiffening). Gelatin methacryloyl (GelMa) was polymerized by differential UV exposure with transparency gradient photomask in 3D printed mold and various gradient strengths were achieved by changing UV exposure time (energy), gradient range of photomask, and GelMa concentration. Human adipose- derived stem cells were cultured on (for 2D) polymerized stiffness gradient GelMa or encapsulated (for 3D) within GelMa with stiffness gradient and.

Results: Using this platform, we discovered that all three mechanomarkers (Lamin A, YAP, and MRTFa) and both sizes of cells and nuclei showed positive relation to stiffness on 2D, however, the trends were opposite in 3D. Cell spreading was controlled by pore size in 3D and it resulted inverse relationship with stiffness.

Conclusion: This platform provides all-in-one system that enables direct comparison between stiffness and mechanomarkers, morphology, and others in 2D and 3D. On-demand stiffening can also add insight in spatiotemporal changes in mechanotransduction in 4D that will further mimic tissue microenvironment.

Improving chondrogenesis of equine umbilical cord blood-mesenchymal stem cell in three-dimensional hydrogel by synergistic control of chemical and mechanical cues

Xiaolin Cui¹, Mitch Durham¹, Jun Li¹, Ellison Aldrich², Khoon Lim¹ and Tim Woodfield¹

¹*Christchurch Regenerative Medicine and Tissue Engineering (CReaTE) Group, Department of Orthopaedic Surgery & Musculoskeletal Medicine, University of Otago, Christchurch, New Zealand, 8011*

²*School of Veterinary Science, Massey University, Palmerston North, New Zealand, 4442*

Introduction: Umbilical cord blood-mesenchymal stem cells (UCB-MSC) have attracted interest due to their multilineage differentiation ability, low immunogenicity and immunomodulatory effect¹. Furthermore, cell sources from UCB can reduce graft rejection and post-transplant infections², and hence are favourable for regenerative medicine applications. However, the impact of mechanical cues such as stiffness, and chemical cues such as signalling molecules, on chondrogenesis of UCB-MSCs in a three dimensional (3D) environment still remains unclear. Therefore, we aim to systematically evaluate the effect of both mechanical and chemical cues on chondrogenesis of UCB-MSCs within a versatile hydrogel matrix.

Method: A visible light crosslinked hydrogel system composed of gelatin-methacryloyl (GelMA) was used to encapsulate UCB-MSC (10 million cells/mL)³. Mechanical cues were tailored by changing the macromer concentration of GelMA (10, 15, 20wt%), whereas chemical cues were introduced by covalently incorporating thiolated heparin (HepSH)⁴. The cell-laden constructs were cultured in chondrogenic media for up to 35 days for maturation before analysis including GAG/DNA, histology, immunohistochemistry (IHC), real-time polymerase chain reaction (PCR) and mechanical testing.

Results: UCB-MSCs showed enhanced chondrogenic capacity in 10% GelMA (26kPa), with confirmation by the improved expression of glycosaminoglycan (GAG), Collagen II and aggrecan, as compared to 15% (35KPa) and 20% GelMA (42KPa). The amount of tissue formation in 10% GelMA was further enhanced by the introduction of HepSH, where the overall GAG production increased to 150 ug/ug.

Conclusion: Synergistic delivery of both chemical and mechanical cues is required for optimal chondrogenesis of UCB-MSC in a 3D hydrogel microenvironment.

References:

1. Sibov, T. T.; Severino, P.; Marti, L. C.; Pavon, L. F.; Oliveira, D. M.; Tobo, P. R.; Campos, A. H.; Paes, A. T.; Amaro, E.; F Gamarra, L.; Moreira-Filho, C. A., Mesenchymal stem cells from umbilical cord blood: parameters for isolation, characterization and adipogenic differentiation. *Cytotechnology* 2012, 64 (5), 511-521.
2. Knutsen, A. P.; Wall, D. A., Kinetics of T-cell development of umbilical cord blood transplantation in severe T-cell immunodeficiency disorders. *The Journal of allergy and clinical immunology* 1999, 103 (5 Pt 1), 823-32.
3. Lim, K. S.; Schon, B. S.; Mekhileri, N. V.; Brown, G. C. J.; Chia, C. M.; Prabakar, S.; Hooper, G. J.; Woodfield, T. B. F., New Visible-Light Photoinitiating System for Improved Print Fidelity in Gelatin-Based Bioinks. *ACS Biomaterials Science & Engineering* 2016, 2 (10), 1752-1762.
4. Brown, G. C. J.; Lim, K. S.; Farrugia, B. L.; Hooper, G. J.; Woodfield, T. B. F., Covalent Incorporation of Heparin Improves Chondrogenesis in Photocurable Gelatin-Methacryloyl Hydrogels. *Macromolecular Bioscience* 2017, 17 (12), 1700158.

Renal fibrosis in human kidney organoids

Veronika Sander¹, J. Digby¹ and Alan. J. Davidson¹

¹*Department of Molecular Medicine and Pathology, University of Auckland, New Zealand*

Introduction: Renal fibrosis is a hallmark of chronic kidney disease (CKD), a serious condition that affects ~1 in 10 New Zealanders. Fibrogenesis in the kidney is initiated by a malfunctional repair response to injury to the renal tubules including nephrotoxicity by commonly used drugs. The pathogenesis of such injury involves acute inflammation, oxidative stress and apoptosis of the epithelial cells, and these processes, when persistent, progress to fibrosis/CKD and eventually renal failure. Despite extensive efforts to unravel the cell types and signalling pathways involved in fibrogenesis, treatment options to effectively block fibrosis and prevent renal failure are currently not available.

Methods: With an urgent need for a clinically relevant model of CKD/fibrosis, we have developed a method for efficient mass-production of kidney organoids derived from human induced pluripotent stem cells. The organoids achieve optimal renal tissue by day 14 when their composition closely resembles fetal kidney tissue with presence of blood filtering podocytes, segmented renal tubules, stromal and endothelial cells.

Results: Upon extended culture, our kidney organoids spontaneously develop fibrosis, which manifests in myofibroblast expansion, deposition of collagen and upregulation of pro-fibrotic/pro-inflammatory markers reminiscent of fibrosis in human kidneys. We found that onset and extent of inflammation and fibrosis can be modulated by inducing AKI in the organoids (via exposure to the anti-cancer drug cisplatin), and that inhibition of pathways implicated in fibrogenesis ameliorates the deleterious effects of cisplatin.

Conclusions: With the strong correlation of fibrosis to CKD, targeting fibrosis in the human cell-based kidney organoid model represents a promising approach for developing new treatments for kidney disease.

ABC 11 - Program – DAY 3

Lecture theatre 505-011, Grafton Campus

5th Dec 2018

MBSANZ18 & ABC11 Shared Day on Mechanobiology AA

<p>2.15pm to 3.55pm Session Chairs: Dr Khoon Lim and Dr Carina Blaker</p>	<p>CELL AND TISSUE MECHANICS</p> <p>Invited Speaker Professor Rami Korhonen – University of Eastern Finland, Finland BIOMECHANICAL RESPONSES OF CHONDROCYTES IN HEALTHY AND MENISCECTOMIZED RABBIT KNEE JOINTS</p> <p>Scientific Presentations</p> <ul style="list-style-type: none"> • A XRD study of biomimetically recalcified bovine bone tissue – Lei Zhao (Hokkaido University) • How much force is required to perforate a colon during colonoscopy? – Niels Hammer (University of Otago) • Mildly degenerative structural changes in the fibrillar matrix of cartilage influences the extent of chondrocyte death following impact loading – Joshua Workman (University of Auckland) • Application of 3D printing technology to facilitate and standardize the testing soft tissues – Niels Hammer (University of Otago) • Shock-absorbing ability of damaged vs undamaged equine cartilage-bone – Fatemeh Malekipour (University of Melbourne) • Three-dimensional bulging of the human medial gastrocnemius muscle during isometric contractions in vivo – Robert Herbert (Neuroscience Research Australia)
---	---

A XRD STUDY OF BIOMIMETICALLY RECALCIFIED BOVINE BONE TISSUE

Lei Zhao¹, Masahiro Todoh¹

¹Human Mechanical Systems and Design, Faculty of Engineering, Hokkaido University

INTRODUCTION

Bone is a composite material consisting of a stiff hydroxyapatite-like mineral phase and a flexible organic phase primarily made of type I collagens. The components have extremely different mechanical properties, but together, the biphasic structure provides bone with high rigidity and resistance against fracture.

During the past two decades, various biomimetic mineralization techniques were developed to simulate the natural mineralization process in bone tissue, which is characterized by the formation of intrafibrillar mineral crystals via the amorphous calcium phosphors (ACP) precursor pathway.

The current study employs state of art X-ray diffraction (XRD) technique [1] to investigate the structure and mechanical properties of recalcified bone matrix, prepared using the polymer-induced liquid precursor (PILP) process, at the nano-scale level.

METHOD

Adult (24 months old) bovine femurs sourced from a local farm were used for this study. After removing all soft tissues, cortical bone samples, measuring approximately 15mm by 4mm by 0.15mm (length x width x thickness), were extracted from the mid-diaphysis region. Care was taken during the process to ensure the long axis of the sample is aligned with the femoral shaft. For demineralized and recalcified samples, further chemical treatments were applied following protocols available in the literature. The samples were air dried for 24 hours before being fixed to a pair of disposable aluminum grips using cyanoacrylate glue, and the glue was allowed to cure in room temperature for overnight. The grip-sample-grip module is then mounted into a tensile loading device inside a custom modified XRD system and irradiated (Cu-K α source) before and after loading were applied.

Wide angle (WAXS)/small angle (SAXS) diffraction patterns and macro-level mechanical data were collected simultaneously during the X-ray irradiation process. The XRD patterns and mechanical data were later analyzed using custom developed MATLAB scripts and Excel respectively.

Raman spectroscopy was also used to investigate the compositional changes after the demineralization and recalcification process.

RESULTS

Figure 1 shows representative wide angle and small angle diffraction patterns from natural, demineralized, and recalcified cortical bone samples. In the wide angle data, diffractions from the (002) and (211)/(300) planes were clearly visible in the natural and the recalcified groups, but were almost completely eliminated in the demineralized group; the c-axis of minerals in the natural and recalcified groups were preferentially aligned with the long axis of collagen fibrils. In small angle data, 3rd order diffraction patterns resulted from the typical 67nm collagen periodicity were only visible in the natural group, suggesting that the pattern is somehow related to the intrafibrillar mineral distribution. Mechanical data showed that the restoration of mechanical properties was positively associated with the duration of the recalcification process. Finally, Raman spectroscopy revealed that pure calcium phosphate minerals were formed during the recalcification process.

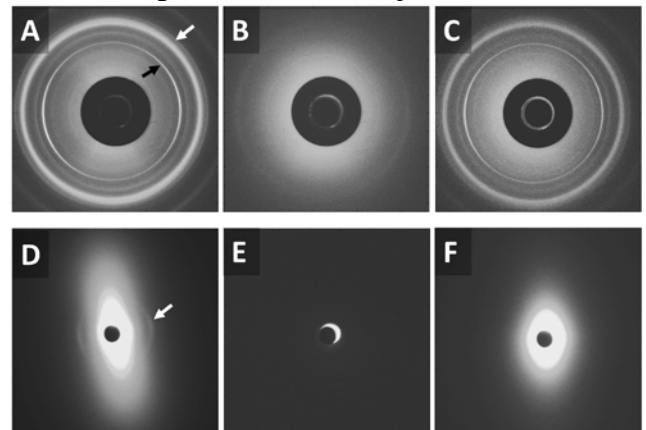


Figure 1. WAXS (top row) and SAXS (bottom row) data from natural (A, D), demineralized (B, E), and recalcified (C, F) samples, showing typical diffraction patterns from (002) (black arrow in A), (211,300) (white arrow in A), and collagen periodicity (arrow in D).

CONCLUSIONS

Biomimetic mineralization is a promising technique for simulating the natural bone mineralization process.

REFERENCES

1. Todoh, M. J. 生体医工学 55Annual (proc), 605-606, 2017

Speaker: Lei ZHAO

Email: leizhao@eng.hokudai.ac.jp

HOW MUCH FORCE IS REQUIRED TO PERFORATE A COLON DURING COLONOSCOPY?

Steve Johnson ^{1,2}, Michael Schultz ^{1,2}, Mario Scholze ³, Troy Smith ³, John Woodfield ⁴, Niels Hammer ^{2,4}

¹ Department of Medicine, Dunedin School of Medicine, University of Otago, Dunedin, New Zealand

² Gastroenterology Unit, Southern District Health Board, Dunedin Hospital, Dunedin, New Zealand

³ Department of Anatomy, University of Otago, Dunedin, New Zealand Department of Anatomy, Dunedin, New Zealand

⁴ Department of Surgical Sciences, Dunedin School of Medicine, University of Otago, Dunedin, New Zealand

⁵ Department of Orthopedic and Trauma Surgery, University of Leipzig, Germany

INTRODUCTION

Colonoscopy is a commonly-performed procedure to diagnose pathology of the larger intestine. Perforation of the colon is a rare but feared complication. It is currently unclear how much force is actually required to cause such injury nor how this is altered in certain diseases. Our aim was to analyze the forces required to perforate the colon in experiments using animal tissues.

METHOD

Using 3D printing technology, models of two commercially available colonoscope heads were 3D printed under three configurations: straight (I), 90°-bent (L) and fully bent (U; Fig. 1). 74 samples of porcine colon were assessed with the models and configurations under perpendicular and angular load application and these data compared to the maximum force typically exerted by experienced colonoscopists.

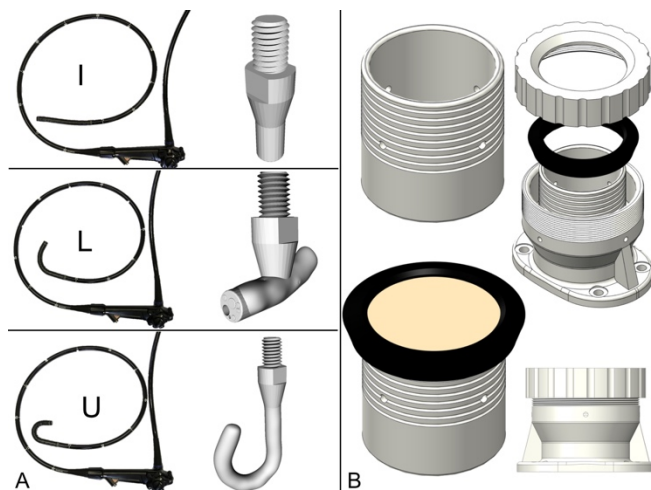


Figure 1. Experimental setup and 3D printed models of commercially available colonoscopes. A: I-, L-, and U-shaped configurations; B: Drum construction for loading colon specimens.

RESULTS

The force required for perforation was significantly smaller for the I compared to the U configuration (23.0 vs. 27.9 N) under perpendicular loading, and for the I compared to the L configuration under angular loading

(14.1 vs. 46.5 N). Similar differences were found for stiffness (I vs. U when loaded perpendicular: 0.65 vs. 1.17 N/m; I vs. L when loaded angular: 0.70 vs. 1.32 N/m). The mode and site of failure varied significantly between the scopes, with delamination of the mucosa/submucosa below the sample (96%) for the I, blunt mucosa/submucosa/muscularis failure adjacent to the loading site (77%) for the L, and failure of all colon layers lateral to the loading site (59%) for the U configuration, respectively. Perpendicular and angulated loading resulted in similar load-deformation values. Maximum forces typically exerted by colonoscopists averaged 13.9 to 27.9 N, depending on the colonoscope model and head configuration.

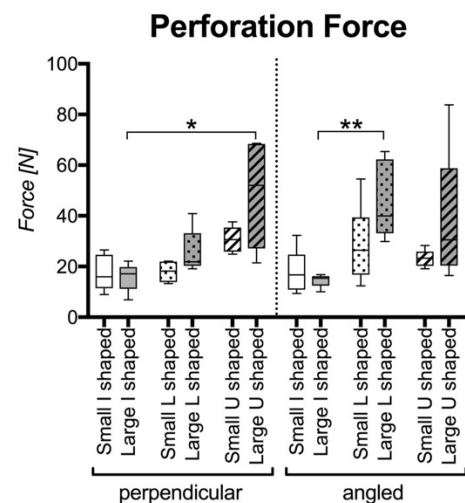


Figure 2: Results from mechanical loading; perforation force.

CONCLUSIONS

The force required for colon perforation varies depending on the type of colonoscope and mode of loading and is likely lower than the force an experienced colonoscopist would exert in daily practice. There is a real risk of perforation, especially when the end of the scope is advancing directly into the colonic wall. The given experimental setup allowed to obtain reliable data of the colon in a standardized scenario, forming the basis for further experiments.

Niels Haammer, nlshammer@googlemail.com

MILDLY DEGENERATIVE STRUCTURAL CHANGES IN THE FIBRILLAR MATRIX OF CARTILAGE INFLUENCES THE EXTENT OF CHONDROCYTE DEATH FOLLOWING IMPACT LOADING

Joshua Workman¹, Neil Broom¹, Ashvin Thambyah¹

¹School of Chemical and Materials Engineering, University of Auckland, New Zealand

INTRODUCTION

We have shown that early fibrillar matrix degenerative changes associated with pre-osteoarthritis do have an influence on the joint response to impact loading [1]. It was found that with mild micro-to-nano scale fibrillar destructuring, while the mechanical response (i.e. peak stress and elasticity of the collision) following impact loading on the cartilage was not different, the structural damage was significantly increased. In this new study we extend the investigation to examine the chondrocyte response of mildly destructured cartilage tissue subject to impact loading.

METHOD

This study utilized the bovine patellae model of osteoarthritis (OA). Six healthy patella (G0) and six patella with grade 1 (G1) degeneration according to the Outerbridge scale [2] were obtained from an abattoir immediately after euthanasia and stored in Dulbecco's Phosphate Buffered Saline with Streptomycin sulfate, kanamycin monosulfate and glucose. Two 15mm square sample blocks were removed from each patellae, one of which was kept aside (as a control), and the other impacted with 2.3J of energy using a vertical drop tower rig and was recorded to evaluate the elasticity of the collision. The peak stress was also recorded using a load transducer. After the impact event a 1mm slice was cut from the center of the sample block and incubated in 5 μ M calcein-AM and propidium iodide at 37°C for 1 hour. These were then examined immediately using an upright laser scanning confocal microscope. Half of each remaining sample was fixed in 10% formalin for 24 hours and then decalcified in 10% formic acid for 3 days. 30 μ m thick cryosections were taken and viewed using differential interference contrast microscopy (DIC), then prepared for scanning electron microscopy (SEM). The percent cell death (PCD) was calculated and used alongside a vulnerability score obtained from damage observed under DIC microscopy as reported previously [1].

RESULTS

The impacts delivered were enough to cause visible damage to the articular surface. Consistent with previous study [1], the peak impact stress and energy absorbed by the collision was not found to be significantly different between the healthy G0 and the

mildly degenerate G1 groups. Similarly to the previous study's finding [1], the mean vulnerability score was significantly increased from healthy to mildly degenerate groups ($p = 0.010$).

Confocal microscopy to measure PCD, showed no significant increase in between the control and the impact groups for healthy G0 samples. On the other hand, the impacted G1 samples had significantly increased PCD compared to their respective controls ($p = 0.014$). Important to note was that the cell death in the impacted G1 tissue extended throughout the full depth of the tissue. There was no significant difference in PCD between G0 and G1 control groups. In the impact groups, there was a significant increase ($p = 0.000$) in PCD (by 260.8%) in the G1 compared to G0. DIC and SEM microscopy confirmed the micro-to-nano fibrillar matrix changes reported in the earlier study [1]. Of interest then were the changes in the peri-cellular matrix (PCM) surrounding the chondrocytes. There was clear evidence that in unimpacted controls the protective basket of the PCM in mildly degenerate tissue was less structurally intact than that found in healthy tissue (Figure 1).

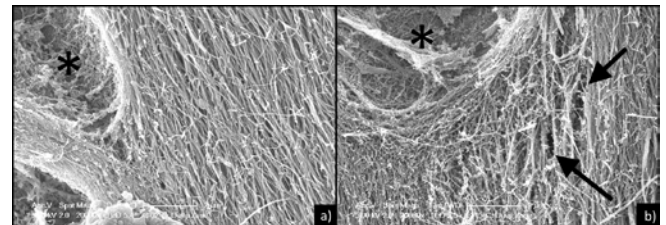


Figure 1: SEM images of the PCM for a) healthy G0 tissue and b) mildly degenerate G1 tissue. Note the excessive disruption of the fibers in the PCM of G1, indicated by the relatively increased porosity in the fiber network (some indicated by arrows). Note the lacuna is where the chondrocyte would have been located (indicated by asterisk).

CONCLUSIONS

In cartilage both the structural and cellular response to impact loading is associated with micro-to-nano scale fibrillar changes in both the ECM and PCM.

REFERENCES

- [1]. Workman et al. Clin. Biomech. 43, 40-49, 2017.
- [2]. Outerbridge. J Bone Joint Surg, 43:B, 752-757, 1961.

Speaker: Joshua Workman

Email: j.workman@auckland.ac.nz

APPLICATION OF 3D PRINTING TECHNOLOGY TO FACILITATE AND STANDARDIZE THE TESTING SOFT TISSUES

Mario Scholze ¹, Aqeeda Singh ¹, Pamela F Lozano ¹, Benjamin Ondruschka ², Maziar Ramezani ³,
Niels Hammer ^{1,4}

¹ Department of Anatomy, University of Otago, Dunedin, New Zealand Department of Anatomy, Dunedin, New Zealand

² Institute of Legal Medicine, Medical Faculty University of Leipzig, Leipzig, Germany

³ Department of Mechanical Engineering, Auckland University of Technology, Auckland, New Zealand

⁴ Department of Trauma, Orthopedic and Plastic Surgery, University Hospital of Leipzig, Leipzig, Germany

INTRODUCTION

Three-dimensional (3D)-printing has become broadly available and can be utilized to customize clamping mechanisms in biomechanical experiments. This study summarizes our preliminary experience using 3D printed clamps to mount soft tissues from different anatomical regions, including. the feasibility and potential limitations of the technology.

METHOD

Tissues were sourced in a fresh condition, including human skin, ligaments and tendons. Clamps with standardized structures and fixtures were 3D printed and used to mount specimens. In quasi-static tensile tests combined with digital image correlation and fatigue trials we characterize the applicability of the novel clamping technique. Scanning electron microscopy was utilized to evaluate the specimens to assess the integrity of the extracellular matrix (ECM) following the mechanical tests.

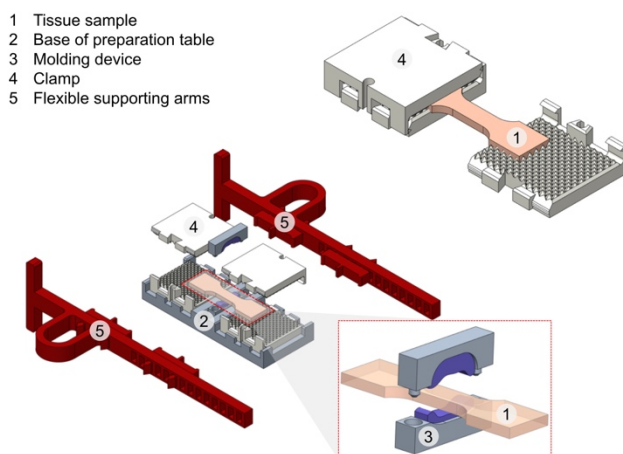


Figure 1. Mounted sample in the self-locking clamps (top right), and schematic representation of the preparation table (center of image) including a (enlarged) molding tool for the determination of cross sections of the samples prior to testing (right bottom).

RESULTS

3D printed clamps showed no signs of clamping-related failure during the quasi-static tests, and intact ECM was found in the area of the clamping, at the transition clamping area and the central area from where the strain data was obtained. In the fatigue tests, material slippage was low, allowing for cyclic tests beyond 10^5 cycles.

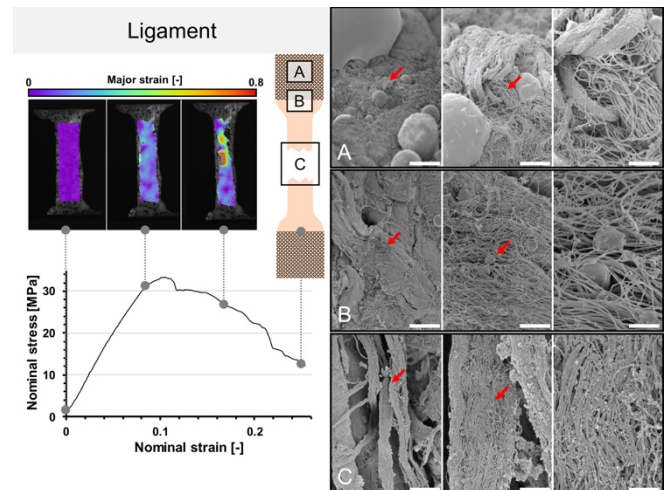


Figure 2: Stress-strain curve of human ligament and the corresponding strain fields from digital image correlation in three steps before the specimen fails. A schematic sample with squares indicates the area where tissues were removed for electron microscopy. Failure of the tissues was observed to different extent at the regions of the testing and clamping, as seen in the inserts A-C.

CONCLUSIONS

Comparison to other clamping techniques yields that 3D printed clamps ease and expedite specimen handling, are highly adaptable to specimen geometries and ideal for highly-standardization and high-throughput experiments in soft tissue biomechanics.

Niels Haammer, nlshammer@googlemail.com

SHOCK-ABSORBING ABILITY OF DAMAGED VS UNDAMAGED EQUINE CARTILAGE-BONE

Fatemeh Malekipour, Chris Whitton, Peter VS Lee
The University of Melbourne

INTRODUCTION

Subchondral bone injury due to accumulation of fatigue microdamage is common in racehorses and athletic humans. The large compressive loads that are repeatedly applied to the joint during racing and training play an important role in the initiation and progression of subchondral bone injury. In the present study, we aimed to compare the shock-absorbing ability and compressive stiffness of subchondral bone from equine third metacarpal (MC3) condyles in specimens with pre-existing microfractures (damaged) and non-damaged specimens.

METHOD

N=17 cartilage-bone plugs (6.5 mm diameter x 10 mm length) were extracted from MC3 condyles of n=8 Thoroughbred racehorses. Plugs were imaged by μ CT at 4 μ m voxel size to identify specimens with microcracks and microfractures which appeared as irregular linear discontinuities in the bone (Figure 1). Specimens were then tested in unconfined compressions perpendicular to cartilage surface. Displacements of 0.191 ± 0.014 mm at 5 Hz were applied to the cartilage surface via a stainless steel compression plate attached to a hydraulic mechanical testing machine (Instron, UK). Overall strain and stress were calculated by dividing the overall displacement and axial force by the overall thickness and cross-sectional area of each specimen, respectively. The linear portion ($R^2 > 0.98$) of the loading curve were specified as the overall stiffness of each cartilage-bone specimen. The area enclosed by the loading-unloading curve of each specimen was specified as the “shock-absorbing ability” or relative energy loss (Eloss) of each specimen [1]. A paired t test was used to compare the stiffness and the Eloss between groups at a significance level of $p=0.05$.

RESULTS

Overall axial stress was 27.6 ± 14.9 MPa for all specimens. Stiffness of damaged and undamaged specimens was 2.69 ± 0.69 GPa and 1.22 ± 0.70 GPa, respectively. Eloss of damaged and undamaged specimens was 48.10 ± 11.49 (%) and 31.02 ± 12.58 (%), respectively. Both stiffness and Eloss were significantly different between damage groups ($p < 0.001$, Figure 2).

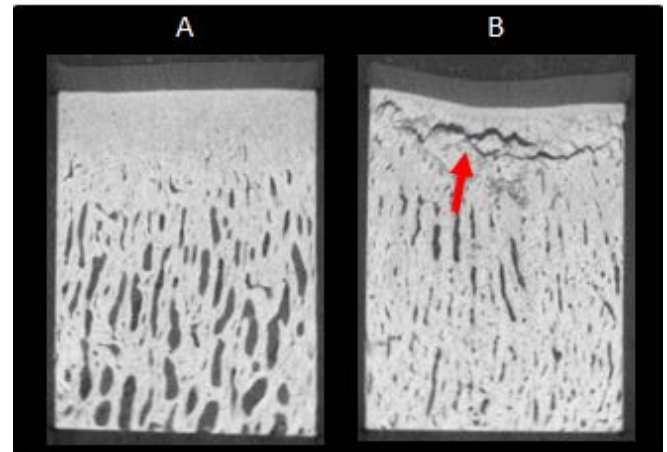


Figure 1: μ CT images of a sagittal cross-section of a typical undamaged (A) and damaged (B) cartilage-bone from distopalmar aspect of the MC3 condyle of a Thoroughbred racehorse.

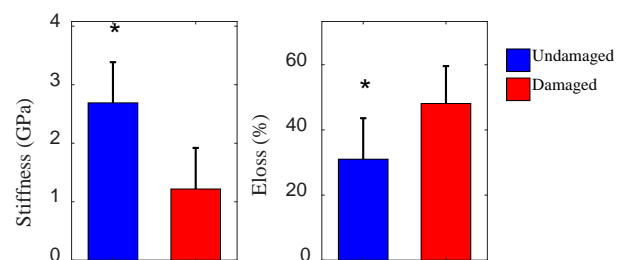


Figure 2. Comparison of stiffness and energy loss between damaged (n=7) and undamaged (n=9) specimens. Error bars indicate the SD of the means. * indicates significance difference between the means.

CONCLUSIONS

The shock-absorbing ability of the pre-existing fatigue-induced microfractures in the subchondral bone may protect its underlying bone from the applied impact load. However, over the long-term, it may also lead to resorption of the underlying bone through blocking of strain transmission. Future investigations will study the correlation between the microstructure and mechanical factors in these specimens to provide better insight into the mechanism of the subchondral bone injury.

REFERENCES

Malekipour, F. J. Mech. Behav. Biomed. Mater. 26, 127–135.

Speaker's name: Fatemeh Malekipour, email address: fmal@unimelb.edu.au.

THREE-DIMENSIONAL BULGING OF THE HUMAN MEDIAL GASTROCNEMIUS MUSCLE DURING ISOMETRIC CONTRACTIONS IN VIVO

Bart Bolsterlee, Martin Héroux and Rob Herbert
Neuroscience Research Australia and University of New South Wales

INTRODUCTION

When muscles contract, they change their shape, i.e. they bulge. Despite the potential relevance of 3D muscle bulging for muscle function [1, 2], little is known about the shape changes that human muscles undergo during contractions *in vivo* as this has been difficult to determine experimentally. Here, we use magnetic resonance imaging (MRI) and shape analysis techniques to measure 3D bulging of the human medial gastrocnemius (MG) during isometric plantarflexion contractions *in vivo*.

METHOD

mDixon MRI scans were obtained from the lower legs of four healthy participants (age 29 ± 4 yrs) when their muscles were relaxed and during plantarflexion contractions at 10% and 20% of their maximum voluntary force. Visual feedback was provided to maintain constant force during the 2.5 minute scan. The scan at 10% contraction was repeated.

3D triangulated surface models with $\sim 10,000$ triangles per model were created of the passive and active muscle using a combination of manual outlining and non-rigid registration. Muscle bulging, here defined as the displacement of the muscle surface in the direction perpendicular to the surface, was measured for each point on the muscle surface by first aligning the contraction model with the model at rest (using principal component analysis), and then calculating the distance of all points on the contraction model to the nearest point on the muscle surface at rest (using a distance map).

Muscle bulging patterns were visually inspected by shading each point on the surface according to how much it bulged inwards (negative) or outwards (positive; Fig. 1). Distributions of inwards and outwards bulging were calculated. For each subject, the absolute-agreement ICC was calculated for bulging values measured at all points on the surface from the first and second scan at 10% contraction.

RESULTS

High quality scans were obtained for all participants and contraction conditions. The MG muscles of all four participants showed similar patterns of muscle bulging during 10% contractions: the central part of the superficial surface, where the superficial

aponeurosis covers the muscle belly, bulged outwards while the sides of the muscle bulged inwards. A reversed pattern was observed during 20% contractions: the central superficial surface bulged inwards, while the sides bulged outwards (Fig. 1). Consistent with the isovolumetric behaviour of muscle tissue, the surface bulged inwards and outwards by similar amounts at both 10% and 20% contractions. At 10% contractions, the mean inwards/outwards bulging was 0.42/0.49 mm (average across subjects) and increased to 0.76/0.83 mm during 20% contractions. The ICC of measurements of muscle bulging at 10% contraction ranged from 0.81-0.88 between subjects.

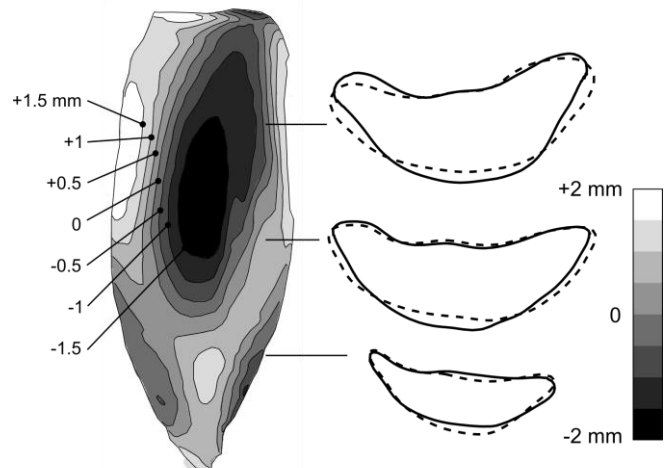


Figure 1. Example of a 3D medial gastrocnemius model (postero-medial view), shaded according to how the muscle bulges during a 20% isometric contraction relative to rest (light: bulge outwards; dark: bulge inwards). Insets show 2D transverse cross-sections at rest (solid line) and during 20% contraction (dashed) at 75%, 50% and 25% of the muscle length.

CONCLUSIONS

We present a novel and reliable method to measure 3D muscle bulging in human muscles *in vivo*. The data presented here may provide novel insights into the active and passive forces that lead to shape changes in contracting muscles, and can be used to validate 3D computational models of muscle contraction.

REFERENCES

- [1] Azizi E PNAS 105, 1745-1750, 2008.
- [2] Stark H, J Biomech 43, 2897-2903, 2010.

Speaker: Bart Bolsterlee (b.bolsterlee@neura.edu.au)

ABC 11 - Program – DAY 3

Lecture theatre 505-011, Grafton Campus

5th Dec 2018

MBSANZ18 & ABC11 Shared Day on Mechanobiology AA

<p>4.20pm to 6.15pm Session Chairs: Dr Lei Zhao and Dr Kelly Burrowes</p>	<p>IMAGING AND MECHANOBIOLOGY</p> <p>Invited Speakers</p> <p>Professor Simo Saaraakala - Oulu University, Oulu, Finland IMAGING OF JOINT TISSUES: IMPLICATION FOR BETTER UNDERSTANDING, DIAGNOSTICS AND PREDICTION OF OSTEOARTHRITIS</p> <p>Professor Martyn Nash – University of Auckland, Auckland, New Zealand REMODELLING OF HEART MUSCLE STRUCTURE AND FUNCTION DUE TO HYPERTENSION</p> <p>Scientific presentations</p> <ul style="list-style-type: none"> • Geometric shape fitting of the tibia and femur in the development of a coordinate system for the knee – Stuart Millar (University of South Australia) • Raman imaging of calcified cartilage and subchondral bone for osteoarthritis research – Shuvashis Das Gupta (University of Oulu) • Parameterisation of diffusion weighted magnetic resonance images of the heart to extract fibre and sheet orientations – Bianca Freytag (University of Auckland) • Investigation of spectral CT for use in bone mineral density assessment and association with histopathological grade – Kenzie Baer (Christchurch Regenerative Medicine and Tissue Engineering Group) • An <i>in-silico</i> model of the extracellular matrix of the lung – Kelly Burrowes (University of Auckland)
---	---

GEOMETRIC SHAPE FITTING OF THE TIBIA AND FEMUR IN THE DEVELOPMENT OF A COORDINATE SYSTEM FOR THE KNEE

¹Stuart Millar, ¹John Arnold, ^{2,3}Lucian Bogdan Solomon, ^{1,3}Dominic Thewlis, ¹Francois Fraysse

¹School of Health Sciences, University of South Australia, SA, AUS; ²Department of Orthopaedics and Trauma, Royal Adelaide Hospital, SA, AUS; ³Centre for Orthopaedic and Trauma Research, University of Adelaide, SA, AUS

INTRODUCTION

Accurate and reliable coordinate system definition is an important element of biomechanical modelling. There have been a number of coordinate systems proposed for the knee utilising medical imaging, often incorporating anatomical landmarks of the tibia and femur [1,2], however, in cases of skeletal trauma the use of anatomical landmarks are somewhat limiting. The aim of this study was to develop a semi-automated method for establishing a coordinate system for the knee to be used for assessing medical imaging data. A geometric shape fitting approach was applied to establish axes for both the tibia and femur from CT reconstructions of the lower limb to form the basis of the coordinate system (CS).

METHOD

CT scans of the lower limb were obtained from 30 healthy adults. Both lower limbs from each scan were manually reconstructed using ScanIP to generate 3D models. The models were imported into Matlab for processing and analysis. Using the full length tibia, a cone was fitted to the outer surface using a least-squares method and the centre of the cone was used to define the longitudinal axis.

To establish the minimum length of shaft required for an accurate axis estimation, further slices were made to the tibial shaft by iteratively discarding 10 mm from the most distal aspect of the shaft and the cone fit applied to increasing smaller lengths of shaft. A reference axis was established from the full length tibia and compared to those axes established at reduced shaft lengths. A similar method was applied to the femur to establish the mediolateral axis using the cone fit for the posterior femoral condyles.

The cross product of the longitudinal axis (Z_T) and mediolateral axis (X_T) were used to define the third axis (Y_T). The origin was defined in the XY plane containing the most distal aspect of the condyles. The AP position of the origin was taken as the intersection of Z_T with this plane, and its ML position as the midpoint of the medial and lateral femoral epicondyles. To assess the repeatability of the axis

estimation, the position of this point was calculated for each shaft length, as a ratio of the tibial plateau depth.

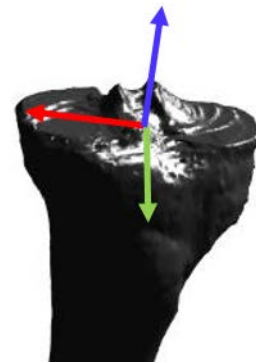


Figure 1. Coordinate system generation.

RESULTS

In estimating the longitudinal axis, angles within the coronal and sagittal plane were within 5° of the reference axis when considering shaft lengths greater than 50 mm. For the mediolateral axis, the smallest deviation from the reference axis occurred at condylar widths greater than 20 mm.

For the origin estimate, its AP position was between 24% and 31% of the tibial plateau depths for shaft lengths between 40-200 mm. Based on the average tibial plateau depth of 57.6 mm, an error of 4 mm was recorded for the axis estimate. The results are based on a preliminary analysis of 10 reconstructed tibiae and femora.

CONCLUSIONS

This study describes a semi-automated method for establishing a CS for the knee. The methodology applied here using a shape-fitting approach to define axes of the tibia and femur shows good accuracy for both the angular deviation and origin estimation, when applied to shaft lengths in excess of 50 mm.

REFERENCES

- Beardsley C, et al. J Biomechanics. 40, 1417-1422, 2007.
- Roos P, et al. J Orthop. Res. 23, 327-333, 2005.

RAMAN IMAGING OF CALCIFIED CARTILAGE AND SUBCHONDRAL BONE FOR OSTEOARTHRITIS RESEARCH

Shuvashis Das Gupta¹, Mikko A. J. Finnilä¹, Rami K. Korhonen², Lassi Rieppo¹, Simo Saarakkala¹

¹University of Oulu, Oulu, Finland. ²University of Eastern Finland, Kuopio, Finland.

INTRODUCTION

Osteoarthritis (OA) is the most common musculoskeletal disease. It leads to degeneration of articular cartilage and sclerosis of the subchondral plate, which is a structure consisting of subchondral bone (SB) and calcified cartilage (CC). However, the separation of these tissue types can be challenging. Thus, the aim of this work is to identify CC and SB and evaluate different biochemical information of both tissue types by using Raman micro-spectroscopy.

METHOD

Cylindrical (d=4mm) osteochondral samples (n=28) were prepared with a dental drill from tibial plateau of cadaveric donors. These samples were further prepared by cutting ~2 mm thick sections, which were submerged in distilled water for Raman imaging. Raman spectral maps were collected with Thermo Scientific™ DXR™2xi Raman Imaging Microscope equipped with a 60x/1.00 water immersion objective and full range grating. To excite Raman signal, 785 nm laser (30 mW) and a 50 μ m confocal pinhole aperture were used, and spectra were collected for 0.5s and averaged for 15 times. All samples were imaged with step sizes of 1 μ m for tidemark and 3 μ m for calcified cartilage and subchondral bone. Pre-processed, vector normalized spectra were fed to K-means clustering analysis. The integrated areas of the $V_4 PO_4^{3-}$ band (543-603 cm^{-1}) and the amide III band (1215-1300 cm^{-1}) were used to calculate mineral-to-matrix ratio as both are less sensitive to the orientation and polarization effect. Carbonate content substitution parameter was investigated by the type-B carbonate symmetric stretch band (1050-1100 cm^{-1}) with respect to $V_4 PO_4^{3-}$ band. Finally, the mineral crystallinity was measured by calculating inverse of the full width at half maximum (FWHM) of $V_1 PO_4^{3-}$ band.

RESULTS

K-means cluster analyses were performed separately on organic vibrations and mineral vibrations (fig 1). When using organic vibrations, SB and CC are separated in distinct clusters, while mineral vibrations seem to separate mineralization front in tidemark to additional clusters. This indicates that CC and bone tissue can be identified from the spectral signature. Univariate analyses of mineral/matrix ratio revealed that CC is significantly more mineralized than subchondral bone tissue (fig 2). Furthermore, Type-B

carbonate substitution and crystallinity indicates SB is more senescent than CC.

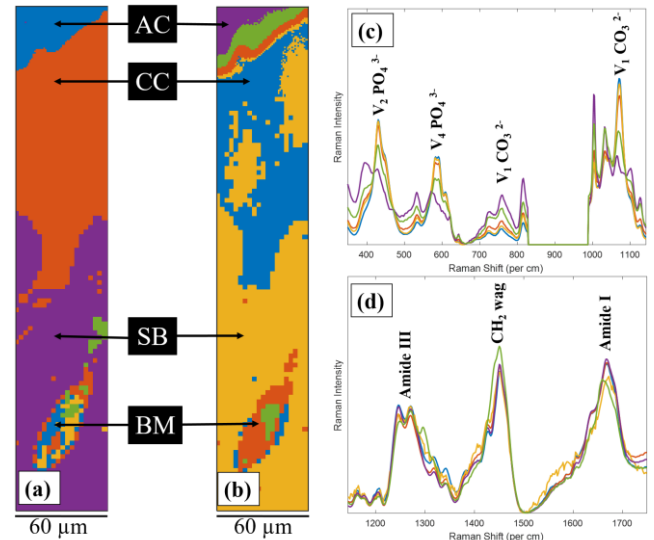


Figure 1. K-means cluster analyses with five clusters using: (a) organic and (b) mineral vibrations, respectively, and (c), (d) mean spectra of both cluster analyses (AC= Articular cartilage, BM= bone marrow).

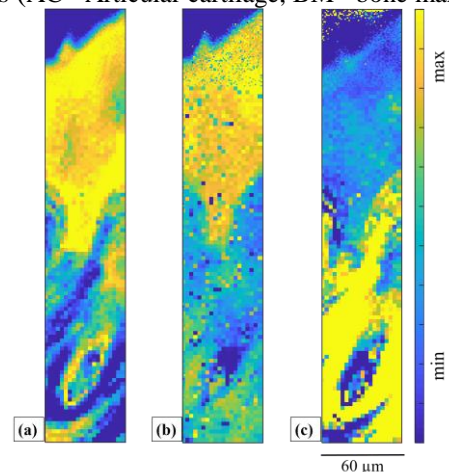


Figure 2. Pseudo-colored univariate images of (a) $V_4 PO_4^{3-}$ / amide III, (b) $(FWHM)^{-1}$ of $V_1 PO_4^{3-}$ band and (c) type-B carb / $V_4 PO_4^{3-}$ respectively.

CONCLUSIONS

In this Raman micro-spectroscopic study, both CC and bone tissue were successfully identified from Raman spectra using K-means cluster analysis. Our results showed that CC is more mineralized and less senescent than bone tissue. This method can be used to provide further insight into tissue-specific biochemical changes in rheumatoid arthritis and osteoarthritis.

Shuvashis Das Gupta, shuvashis.dasgupta@oulu.fi

PARAMETERISATION OF DIFFUSION WEIGHTED MAGNETIC RESONANCE IMAGES OF THE HEART TO EXTRACT FIBRE AND SHEET ORIENTATIONS

Bianca Freytag¹, Vicky Y. Wang¹, G. Richard Christie¹, Gregory B. Sands^{1,2}, Ian J. LeGrice^{1,2},
Alistair A. Young^{1,3}, and Martyn P. Nash^{1,4}

¹ Auckland Bioengineering Institute, University of Auckland (UoA) - ² Department of Physiology, UoA

³ Department of Anatomy with Radiology, UoA - ⁴ Department of Engineering Science, UoA

INTRODUCTION

This study presents a workflow for parameterising myocardial fibre and sheet orientations of the left ventricle (LV) from diffusion tensors without the need to perform eigenanalysis of diffusion tensors. This fitting approach is an alternative to eigenanalysis as it avoids issues of ambiguous eigenvector directions and the non-uniqueness of eigenvectors in regions of isotropic diffusion.

It is well established that the direction of maximal diffusion aligns with the cardiac myofibre orientation. The direction of minimal diffusion is hypothesised to correlate with the sheet normal direction, as diffusion of water molecules across sheets is likely to be restricted¹. This study extends a previous framework² to also parameterise sheet-normal orientations.

METHOD

Finite element (FE) parameters describing the spatially varying fibre and sheet-normal orientations throughout the LV are directly fitted to diffusion tensors using non-linear least squares optimisation.

A geometric 16-element tricubic-Hermite LV FE model was fitted to the segmented endocardial and epicardial surfaces of an *in-vivo* pig heart¹ using non-linear least squares. From 6 diffusion-weighted signals, the diffusion tensors were pre-calculated for each voxel by solving the logarithm of the diffusion equation proposed by Basser et al.³

The FE fibre field was initialised by setting the fibre angles ($\theta_{(n)}$) to be +60° for the endocardial nodes, and -70° and the epicardium. Initial imbrication ($\phi_{(n)}$) and sheet-normal ($\psi_{(n)}$) angles of all nodes were set to 0° (sheet-normal axes pointing orthogonal to the wall plane). For each voxel a set of local orthogonal material axes $\mathbf{f}_{(v)}$ (fibre), $\mathbf{s}_{(v)}$ (sheet), and $\mathbf{n}_{(v)}$ (sheet-normal) were interpolated over the FE model using tricubic Hermite basis functions.

The two scalar objective function (Δ_f , Δ_n) were:

$$\Delta_f = \sum_v \mathbf{f}_{(v)}^T \cdot \mathbf{D}_{(v)} \mathbf{f}_{(v)} \text{ and } \Delta_n = \sum_v \mathbf{n}_{(v)}^T \cdot \mathbf{D}_{(v)} \mathbf{n}_{(v)}.$$

At a given voxel, if $\mathbf{f}_{(v)}$ and the direction of maximal diffusion were perfectly aligned, then Δ_f , defined as the dot product of $\mathbf{f}_{(v)}$ with the projection of the diffusion tensor ($\mathbf{D}_{(v)}$) in the direction of $\mathbf{f}_{(v)}$, would be maximal. Conversely, Δ_n would be minimal if $\mathbf{n}_{(v)}$ was

aligned with the direction of minimal diffusion. Finally, Δ_f was maximised and Δ_n minimised using nonlinear optimisation (least-squares quasi-Newton) by modifying the nodal parameters $\theta_{(n)}$ and $\psi_{(n)}$.

RESULTS

The alignment between estimated fibre orientations and primary eigenvectors was generally good, especially in areas of high diffusion anisotropy (mean difference between primary eigenvector and $\mathbf{f}_{(v)}$: 3.1°). However, largely varying tertiary eigenvectors suggest that there may be more than one family of sheets present; the fitting is not able to represent both families simultaneously. Agreement between tertiary eigenvectors and $\mathbf{n}_{(v)}$ is good in regions of high anisotropic diffusion, but poor where the diffusion appears more isotropic (mean difference: 13.7°).

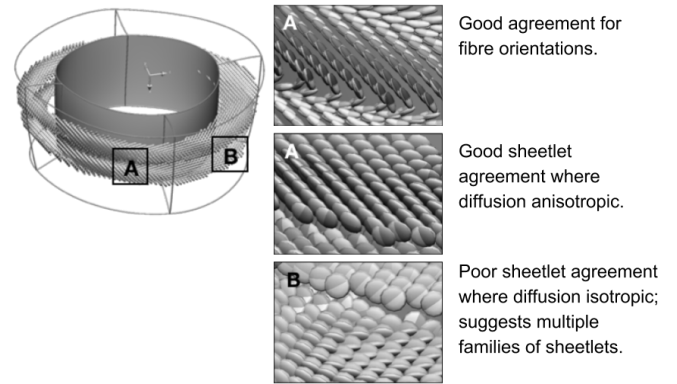


Figure 1. Fibre and sheetlet fitting result

CONCLUSIONS

A field-based parameterisation scheme was developed to extract both fibre and sheet-normal orientations from diffusion weighted MRI data. It does not require the calculation of primary and tertiary eigenvectors. Results showed good alignment for fibre orientations, but suggest that a single field for sheet-normal orientations may not be sufficient in regions with multiple families of sheetlets. In future, this framework will be used to construct geometric FE models for individualised analyses of heart mechanics.

REFERENCES

1. Nilles-Vallespin, J Am Coll Cardiol, 69(6):661–676, 2017.
2. Freytag, LNCS 9126, 146–154, 2015.
3. Basser, J Magn Reson B 103(3), 247–254, 1994.

Presenter's name: Bianca Freytag, b.freytag@auckland.ac.nz

INVESTIGATION OF SPECTRAL CT FOR USE IN BONE MINERAL DENSITY ASSESSMENT AND ASSOCIATION WITH HISTOPATHOLOGICAL GRADE

K. Baer¹, S. Kieser¹, A. Raja¹, T. Woodfield¹

(1) University of Otago, Christchurch, NZ

INTRODUCTION

Osteoarthritis (OA) severity can be characterized by degradation of cartilage as well as changes in microstructure and decreased bone mineral density (BMD) of subchondral bone¹. It has been shown that altered subchondral bone can cause biomechanical changes in the joint creating an additional factor in OA progression². Current established grading methods do not incorporate these subchondral bone changes into the criteria until the later stages of OA³. Dual X-ray Absorptiometry (DXA) is used to assess BMD but it is limited to a two dimensional area bone assessment and lacks the ability to image soft tissue. Spectral CT has the ability to scan with multiple energy ranges and separate materials based on attenuation, which can be utilized to quantify hydroxyapatite (HA) of subchondral bone as well as cartilage health. The purpose of this study was to determine the ability of spectral CT to quantify BMD compared to current techniques and show the connection of subchondral bone BMD to the Osteoarthritis Research Society International (OARSI) assessment system for OA.

METHOD

Six lateral tibial plateaus (4 female age: 61-69, 2 male: age 58) were scanned with DXA and spectral CT using predetermined protocols. Reconstructed spectral CT images underwent material decomposition, separating spectral images into images of lipid, water and HA, with HA images used for analysis of BMD. Regions of interest (ROIs) were determined to mimic DXA ROIs. Volumetric BMD of spectral CT images was calculated using ImageJ. The lateral tibial plateaus were processed for histological analysis. Twenty 5- μ m thick sections were cut, ten were stained with Safranin O-fast green (Saf-O) and ten were hematoxylin and eosin (HE). All sections were scored by two independent researchers according to the OASRI assessment criteria. Spectral CT volumetric BMD and DXA areal BMD were compared to each other and correlated to the OARSI score for each ROI.

RESULTS

In order to detect overall trends in the data, the height of the DXA BMD bars were scaled such that the largest DXA area BMD measurement was aligned with the largest spectral CT volumetric BMD measurement. The BMD for the outer edge (region 1) and middle (region 2) of the lateral tibial plateau from

spectral CT are proportionate to DXA BMD. The spectral CT BMD for the inner edge of the lateral plateau are below the DXA BMD (Figure 1A). The Spearman Rank Correlation shows a strong association between spectral CT and DXA BMD ($R = 0.72$). The correlation between DXA area BMD and OARSI score and spectral CT volumetric BMD and OARSI score both show a negative correlation as expected (Figure 1B). Neither imaging modality showed a strong correlation to the OARSI score.

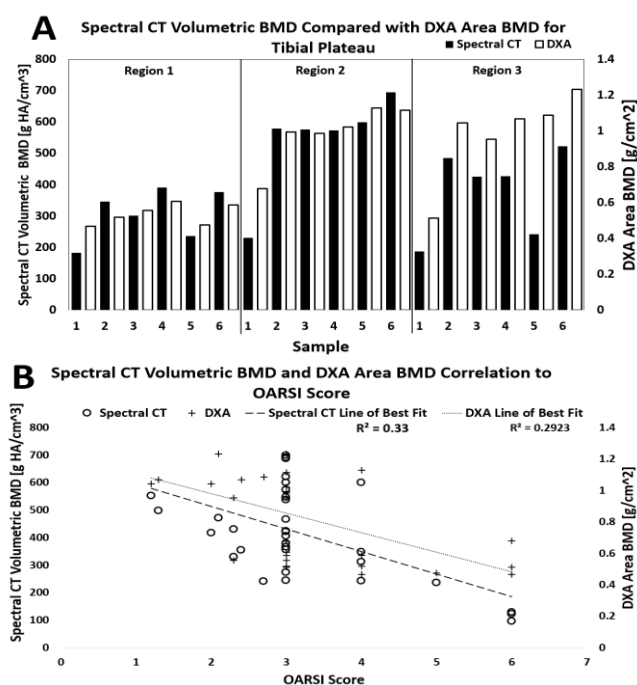


Figure 1. (A) DXA area BMD compared to spectral CT volumetric BMD (B) correlation graph for BMD to OARSI score.

CONCLUSIONS

Spectral CT can provide site specific BMD analysis corresponding to current techniques used to assess bone health. While we do see the inverse relationship between BMD and OARSI score, the poor correlation highlights the lack of inclusion of subchondral bone into the OARSI assessment system.

REFERENCES

- [1] Lee, JY. Arthritis Rheum.65, 1541-1546,2013.
- [2] Finnila, M.A.J. B. J. Othop. Res.35, 785-792, 2017.
- [3] Hardcastle, S. BoneKey. 4, 624, 2015.

Kenzie Baer – kenzie.baer@postgrad.otago.ac.nz

An in-silico model of the extracellular matrix of the lung

Kelly Burrowes¹, Amin Iravani¹ and Ashwin Thambyah¹

¹*Department of Chemical and Materials Engineering, University of Auckland, Auckland, New Zealand*

Introduction: The mechanical properties of lung tissue are largely determined by the structure and composition of the extracellular matrix (ECM). Changes in the ECM have been linked with the pathology of many respiratory diseases. For example, Chronic Obstructive Pulmonary Disease (COPD) involves emphysema (loss of elastin) and chronic bronchitis (remodelling of the airways). In this study, we have developed a spring network model of the lung ECM to investigate the impact of these changes on resultant stress distribution.

Methods: Our network model specifically represents collagen, elastin and proteoglycans (PGs). The collagen-PG system is represented using a non-linear spring in parallel with a Maxwell-type model, providing viscoelastic properties. Stability is added to the hexagonal spring system via diagonal springs representing PGs. A vertical spring with high compliance is included within each hexagon to represent elastin. We varied the properties of the network model to mimic changes in the ECM during disease. We added airways, with varying stiffness, to investigate the impact of these on the stress distribution within the tissue during an in-silico uniaxial tensile test.

Results: The model is able to predict physiologically-consistent stress-strain curves in healthy lung tissue. By removing vertical springs, representing elastin, we were also able to predict stress-strain curves that matched well with measurements in emphysematous lung tissue. Incorporating airways into the ECM model and stiffening those airways impacted on the resultant stress-strain curve of the tissue and increased stress heterogeneity within individual springs in the network.

Conclusions: Our model is able to mimic lung ECM and will be applied to understand the impact of ECM alterations during pathology.